10.1515/msr-2015-0037

Novel Method for Sizing Metallic Bottom Crack Depth Using Multi-frequency Alternating Current Potential Drop Technique

Yuting Li, Fangji Gan, Zhengjun Wan, Junbi Liao and Wenqiang Li

School of Manufacturing, Science and Engineering, Sichuan University, Chengdu, Sichuan province, 610065, P. R. China.
scucklyt@163.com, wanzj1987@qq.com

Potential drop techniques are of two types: the direct current potential drop (DCPD) technique and alternating current potential drop (ACPD) technique, and both of them are used in nondestructive testing. ACPD, as a kind of valid method in sizing metal cracks, has been applied to evaluate metal structures. However, our review of most available approaches revealed that some improvements can be done in measuring depth of metal bottom crack by means of ACPD, such as accuracy and sensitivity of shallow crack. This paper studied a novel method which utilized the slope of voltage ratio-frequency curve to solve bottom crack depth by using a simple mathematic equation based on finite element analysis. It is found that voltage ratio varies linearly with frequency in the range of 5–15 Hz; this range is slightly higher than the equivalent frequency and lower than semi-permeable frequency. Simulation and experiment show that the novel method can measure the bottom crack depth accurately.

Keywords: Nondestructive testing, alternating current potential drop technique, bottom crack, depth measurement.

1. INTRODUCTION

IT IS WELL KNOWN that defects often form in metal structures during the service period. Corrosion, stress, fatigue and flaws in manufacturing stage may contribute to these defects. Therefore, defect detection is necessary in avoiding huge losses of lifespan and property that may be caused by those defects. For a variety of defects, bottom cracks caused by stress and fatigue are often hidden and dangerous. Present techniques for detecting bottom cracks, such as eddy current [1], [2], alternating current field measurement (ACFM) [3], and ultrasonic techniques [4] are used. As one of the nondestructive testing (NDT) techniques, potential drop technique has been used widely.

According to excitation current type, potential drop technique can be classified into direct current potential drop (DCPD) technique and alternating current potential drop (ACPD) technique. The former is more suitable for monitoring initiation and orientation of cracks, while the latter is mainly used for sizing cracks on a metal upper surface [5-8]. The advantage of the ACPD over DCPD is that lower excitation current supplies sufficient amplitude of potential drop, which reduces the accident risks in application [9]. Furthermore, the measuring results of ACPD have higher sensitivity and anti-interference ability in comparison with DCPD. Additionally, ACPD technique is also used in measuring properties of metallic materials [10]. However, ACPD is seldom used in sizing bottom crack, and in most cases, the flaws on metal surface (upper and bottom) are evaluated through analyzing a pair of voltages in ACPD, which may obtain insufficient information for solving flaw size. With the aim of finding a better approach in sizing bottom crack, the current redistribution cause of crack was investigated. Moreover, the slope of voltage-frequency curve was used as the main parameter to evaluate crack depth.

2. ACPD PRINCIPLE

Alternating current (AC) distribution follows skin effect [11] in good conductors. High frequency current flows on the metal top and bottom surfaces and the current flowing part is a layer of current penetration depth δ under the entire surface of the conductor [12], whereas lower frequency current may penetrate the entire conductor. The skin depth δ depends on the current frequency f and metal properties and is given by:

$$\delta = \frac{1}{\sqrt{\pi \mu_r \mu_0 \sigma f}} \tag{1}$$

where $\mu_0 = 4\pi \times 10^{-7}$H/m is the magnetic permeability of vacuum, μ_r is the relative magnetic permeability, and σ is the electrical conductivity.

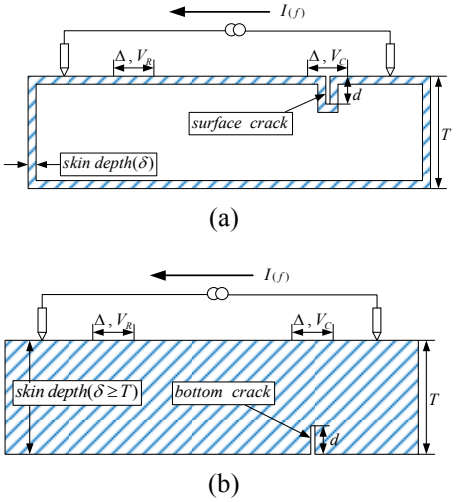

Fig.1. a) Schematic description of surface crack detection using ACPD. b) Schematic description of bottom crack detection using ACPD.

Fig.1.a) shows that when a surface crack with depth d exists, redistribution current flows along the crack profile [13]. Moreover, the crack causes additional current path and a larger potential drop [14]. $I_{(f)}$ is the AC excitation current with frequency f, and Δ is the distance between each pair of electrodes. V_C and V_R are the voltages in the cracked and the undamaged regions, respectively. V_R is used as the reference voltage. When f increases, V_C and V_R increase as well. In the high frequency excitation situation, δ is very small, so surface crack depth can be assessed by analyzing V_C/V_R with the thin & thick model as proposed by Saguy and Rittel [8].

As shown in (2), f_{DC} is a threshold of quasi direct current situation, and any frequency which is lower than f_{DC} can use the DCPD method to detect cracks. In general, with enhanced penetration of current, the frequency is decreased to $f < f_{DC}$ to detect the bottom crack in recent years. Under this frequency condition, the effect of magnetic permeability on measurement can be neglected [10], V_C and V_R are constant with f decreasing continuously, and the alternating current distributes evenly over the entire conductor [15] as shown in Fig.1.b). The analytical ACPD method for bottom crack detection is equivalent to the DCPD method, however, crack initiation and growth monitoring have been the analytical emphasis in DCPD [16], [17], and the accuracy of crack depth measurement has been seldom mentioned. Furthermore, traditional potential drop methods use only one pair of voltages (V_C and V_R) to estimate the crack depth, which is a reason for limitation of accuracy. This paper emphasizes frequency range over f_{DC}, and takes magnetic permeability into consideration.

$$f_{DC} = \frac{\sqrt{45}}{20\pi\mu_r\mu_0\sigma T^2} \tag{2}$$

Multi-frequency alternating current potential drop (MACPD) technique as an extension of ACPD technique has been used to test surface cracks in metal cylinders [18] and bottom cracks in thick metal plates [19] (width ≥ 0.5 T). A relationship has also been identified between the skin depth δ and the uncracked thickness (t–d) [20]:

$$\frac{\delta}{(t-d)} = 0.5 \tag{3}$$

As we can see, equations (1) and (3) are simple, and equation (3) contains a crucial parameter, δ, which depends on relative magnetic permeability μ_r and electrical conductivity σ. Therefore, μ_r and σ should be measured accurately in advance to ensure precision in bottom crack measurement. Because of the nonlinear relationship between δ and f, the penetration depth δ changes more rapidly with f at low frequency than at high frequency. So, it is inconvenient to search for a certain frequency that will satisfy equation (3) well when d is very small.

To obtain more voltages for bottom crack depth evaluation, a multi-frequency approach based on a certain frequency range that is slightly higher than f_{DC} and lower than f_{SP} (as in (4)) has been used. f_{DC} is equivalent frequency, and f_{SP} is semi-permeable frequency when $\delta = T/2$.

$$f_{SP} = \frac{4}{\pi\mu_r\mu_0\sigma T^2} \tag{4}$$

3. Analysis

COMSOL Multiphysics modeling software (COMSOL Inc., Stockholm, Sweden) is a finite element method (FEM) tool for theoretical electromagnetic (AC/DC module) simulation calculations [21]. Fig.2. shows the thin metal plate simulation model with properties as listed in Table 1. Ω is the solution domain, S_1 and S_2 are the current excited boundaries, and S_3 represents all boundaries except S_1 and S_2. Δ is the distance between two electrodes. C is a crack with depth d, and is perpendicular to bottom and front surface. V_C is the voltage of the crack upper surface, and V_R is the reference voltage. As the non-linear relation between material magnetic permeability and excitation frequency, which may alter the predicted V_R and V_C values, it is assumed that magnetic permeability is a constant.

Table 1. Current amplitude, properties and model dimensions.

I/A	μ_r	σ/MS	Δ/mm	L×W×T/mm^3
2	110	5.5	20	500×200×10

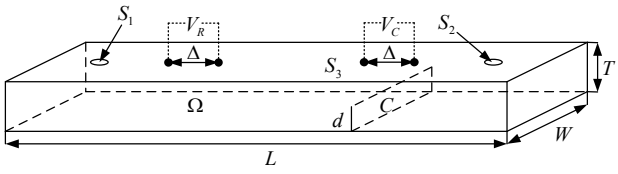

Fig.2. COMSOL simulation model.

At low frequency, the displacement current can be neglected ($\sigma >> \omega\varepsilon$, where ω is angular frequency and ε is permittivity). If we suppose that the excitation current varies sinusoidally with time, the real part of $\exp(j\omega t)$ can be represented by:

$$\tilde{\boldsymbol{I}}(\boldsymbol{r}) = I(\boldsymbol{r})e^{-j\omega t} \tag{5}$$

where $j = \sqrt{-1}$ and $\boldsymbol{r}$ is the position vector in spherical coordinates. Ω depends on the following governing equations:

$$\nabla V(\boldsymbol{r}) = -\tilde{\boldsymbol{E}}(\boldsymbol{r}) - j\omega\tilde{\boldsymbol{A}}(\boldsymbol{r}) \tag{6}$$

$$\nabla^2\tilde{\boldsymbol{J}}(\boldsymbol{r}) - j\omega\mu\sigma\tilde{\boldsymbol{J}}(\boldsymbol{r}) = 0 \tag{7}$$

$$\nabla^2\tilde{\boldsymbol{A}}(\boldsymbol{r}) = -\mu\tilde{\boldsymbol{J}}(\boldsymbol{r}) \tag{8}$$

The boundary conditions are:

$$S_1 : -\boldsymbol{n}\cdot\tilde{\boldsymbol{J}} = I / S_1, \tag{9}$$

$$S_2:\ \boldsymbol{n}\cdot\tilde{\boldsymbol{J}} = I/S_2,\ \boldsymbol{n}\times\tilde{\boldsymbol{A}} = \boldsymbol{0} \qquad (10)$$

$$S_3:\ \boldsymbol{n}\cdot\tilde{\boldsymbol{J}} = 0,\ \boldsymbol{n}\times\tilde{\boldsymbol{A}} = \boldsymbol{0} \qquad (11)$$

$\tilde{\boldsymbol{A}}(\boldsymbol{r})$ is the magnetic vector potential, $\tilde{\boldsymbol{E}}(\boldsymbol{r})$ is the electric field strength, $V(\boldsymbol{r})$ is the scalar voltage potential, $\tilde{\boldsymbol{J}}(\boldsymbol{r})$ is the current density, and $\boldsymbol{n}$ is the boundary normal vector.

Substituting the values in Table 1. into (2) and (4), we can obtain equivalent frequency (f_{DC} = 1.4 Hz) and semi-permeable frequency (f_{SP} = 16.75 Hz), respectively.

The current density can be determined from (6) to (11). For instance, when f = 10 Hz and d = 4 mm, the current distribution of the plate plane is shown in Fig.3.a), where a color change from blue to red indicates a current increase. In the undamaged region (Fig.3.b)), the current density near top and bottom surfaces is slightly higher than that of inner surface, whereas, when a bottom crack appears (Fig.3.c)), the current distribution changes greatly near the crack tip and causes an obvious increase in density on the upper surface. Furthermore, the corner effect on the bottom surface is apparent.

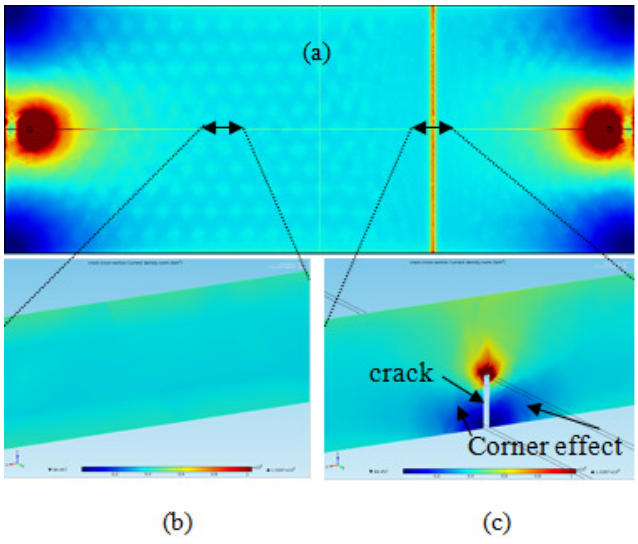

Fig.3. Simulation result in undamaged and crack area, for f = 10 Hz, d = 4 mm.

The above case suggests that various frequencies ($f_{DC} < f < f_{SP}$) lead to unlike redistribution current at the crack tip. So it is a conclusion that the relation between various frequencies and values of V_C/V_R can supply some help in accurate measurement of bottom crack depth.

By means of multiple simulations, the relation between V_C/V_R and f was obtained and four cases were given. The ratio of bottom crack depth to specimen thickness, slope of line fitting curve k, coefficient of determination R^2 for four cracks with different depths (V_C/V_R–f curves in Fig.4.) are shown in Table 2.

Table 2. Slope k and coefficient of determination R^2.

d/T	$k/10^{-3}$	R^2
0.2	-3.034	0.9995
0.4	-8.554	0.9995
0.6	-17.179	0.9993
0.8	-29.306	0.9987

It is obvious to find that the four curves in Fig.4. are extremely similar to straight lines, and the $R^2 \approx 1$ shown in Table 2. confirms the linear relation between V_C/V_R and f in the frequency range of 5–15 Hz. Since one depth has only one corresponding k, it can be used to calculate the bottom crack depth d. In order to simplify data analysis, K, as the inverse of slope k, is used as x-axis variable in fitting curve. The d–K curve (Fig.5.) is obtained through nonlinear fitting, with 17 representative simulation data for comparison. The formula that relates d and K is given by:

$$d = 4.3\ln(1000K + 5.6) - 7.41 \qquad (12)$$

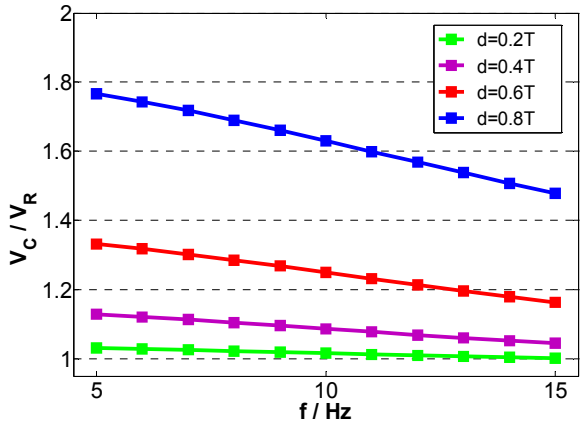

Fig.4. V_C/V_R –f fitting curve for 5–15 Hz.

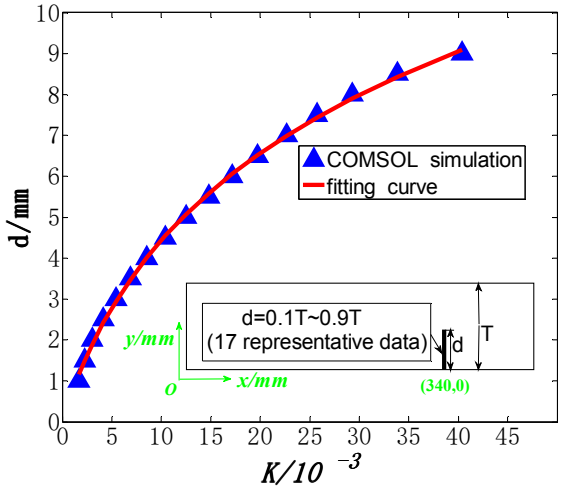

Fig.5. d-K simulation data and fitting curve.

4. EXPERIMENT

To verify the accuracy of the new method proposed, experiments were conducted with setup shown in Fig.6. A AISI 1045 carbon steel plate and a 65 Mn spring steel plate were selected as the test specimens. The specimens, their magnetic, electrical properties, and dimensions are summarized in Table 3.

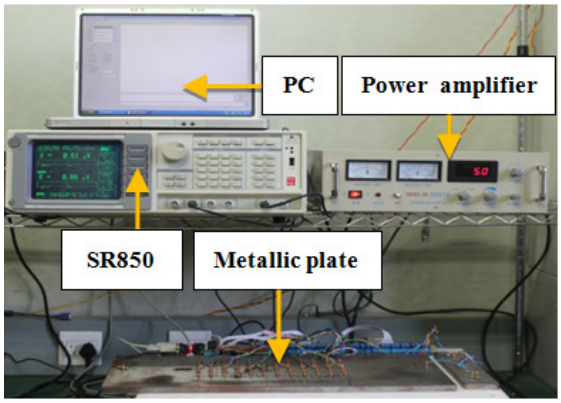

Fig.6. Metallic plate set-up.

Table 3. Materials, properties, dimensions of the specimens.

Set	Materials	μ_r	σ/MS	L×W×T/mm
Plate1	AISI 1045	110	5.5	500×200×10
Plate2	65Mn	90	5.3	500×200×9

An *SR850* (Stanford Research System, CA, USA), which was a digital lock-in amplifier with voltage measurement accuracy of 2 *nV*, and also supplied the source signal for the power amplifier, was used to process the measured weak signal in the experiment. The power amplifier can provide a maximum sinusoidal current of 5 amperes and an excitation frequency range of 0.5 Hz – 10 kHz. A personal computer (PC) was used for data recording and analyzing.

Before measurements, five different cracks, three cracks were on plate1 and two cracks were on plate2, perpendicular to the bottom and front surfaces, were introduced in different regions to be measured on the bottom surfaces of plates. The cracks were made using *Super MM50A* (Seibu Electric & Machinery Co., Ltd., Fukuoka, Japan), which was a high-precision submerged type wire electric discharge machine (EDM) with machining precision of ±1 μm, and the maximum processing width was less than 0.5 mm. As shown in Fig.7., five cracks, C*i* (*i* =1, 2, 3, 4, 5), with depth of 2 mm, 4 mm, 6 mm, 5 mm and 7 mm, were manufactured in plate1 and plate 2, respectively.

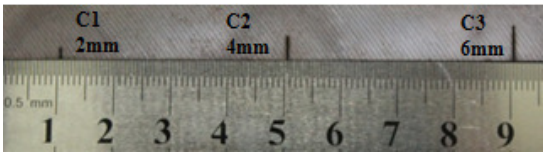

(a)

(b)

Fig.7. Wire EDM machining cracks on bottom surfaces of measured plates: a) cracks on plate1, b) cracks on plate2.

In Fig.8. a measurement area (undamaged or cracked) was obtained with each pair of electrodes separated by a distance of 20 mm. Current was injected at points on the symmetry axis along the lengthwise direction; these points were sufficiently far from the measurement areas. It was thus ensured that the lines between electrodes and injected points were collinear, and the current flowed fairly evenly before reaching the measurement areas. The locations of five cracks and reference electrode are listed in Table 4.

Table 4. Locations of cracks and reference electrodes.

Set	Crack series	x_c/mm	x_r/mm
Plate1	C1	160	150
	C2	200	
	C3	240	
Plate2	C4	200	190
	C5	250	

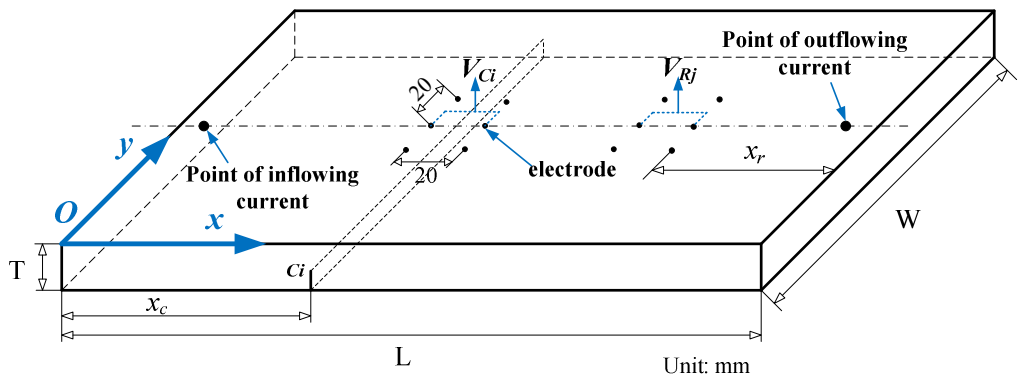

Fig.8. Schematic description of the crack configuration.

When power amplifier provided sinusoidal current with an amplitude of 2 A from 5 to 15 Hz in 1 Hz intervals, the voltage in each cracked area was given as V_{Ci} (i =1, 2, 3, 4, 5), and the reference voltage in each plate was given as V_{Rj} (j =1, 2). So 7 series of voltages were measured in experiment and the results are given in Table 5.

Table.5. Measured voltages from 5–15 Hz.

f/Hz	Plate1			Plate2			
	Unit: μV						
	V_{C1}	V_{C2}	V_{C3}	V_{R1}	V_{C4}	V_{C5}	V_{R2}
5	4.232	4.625	5.452	4.087	2.595	3.414	2.040
6	4.307	4.695	5.492	4.173	2.612	3.417	2.045
7	4.361	4.737	5.504	4.237	2.613	3.418	2.073
8	4.455	4.787	5.568	4.316	2.620	3.419	2.114
9	4.522	4.870	5.623	4.429	2.623	3.417	2.147
10	4.641	4.921	5.653	4.519	2.621	3.422	2.162
11	4.721	5.020	5.707	4.632	2.648	3.425	2.192
12	4.830	5.104	5.746	4.748	2.655	3.428	2.218
13	4.924	5.206	5.842	4.885	2.672	3.429	2.249
14	4.999	5.262	5.857	4.986	2.681	3.432	2.282
15	5.111	5.366	5.925	5.100	2.696	3.434	2.316

Table 6. shows the ratios for the given frequency range. The computer used the least square fitting method to analyze the ratios and obtain the K values as the following.

$$K_{C1} = 3.5\times10^{-3},\ K_{C2} = 8.34\times10^{-3},\ K_{C3} = 17.58\times10^{-3}$$
$$K_{C4} = 11.5\times10^{-3},\ K_{C3} = 19.7\times10^{-3}$$

Table 6. Ratio of V_C/V_R from 5–15 Hz.

f/Hz	ratio				
	V_{C1}/V_{R1}	V_{C2}/V_{R1}	V_{C3}/V_{R1}	V_{C4}/V_{R2}	V_{C5}/V_{R2}
5	1.0356	1.1316	1.3342	1.2721	1.6735
6	1.0332	1.1252	1.3162	1.2773	1.6709
7	1.0292	1.1180	1.2989	1.2605	1.6488
8	1.0322	1.1091	1.2901	1.2394	1.6173
9	1.0210	1.0995	1.2694	1.2217	1.5915
10	1.0271	1.0889	1.2508	1.2123	1.5828
11	1.0192	1.0837	1.2320	1.2080	1.5625
12	1.0173	1.0750	1.2104	1.1970	1.5455
13	1.0079	1.0657	1.1958	1.1881	1.5247
14	1.0026	1.0553	1.1746	1.1748	1.5039
15	1.0022	1.0522	1.1619	1.1641	1.4827

Inserting K into (12) yields the measured depth, and the errors were calculated. In Fig.8., the maximum relative error is below 10 % (relative error = 100 % × |measured – actual|/actual), and the error compared with actual plate thickness is found to be below 6 % T. From the measured result it can be found that the errors of crack depth in 65 Mn are slightly more than that in 1045, especially the error compared with actual plate thickness. And the distinction suggests that some other materials, whose permeability largely differs from the AISI 1045 carbon steel, use (12) for depth measurement and may have bigger errors.

In this study, the simulation and experiment focus on magnetic materials and the specific frequency range 5–15 Hz. As the relative permeability of non-magnetic metallic materials such as aluminum and stainless steel are approximately equal to 1, so considering the properties of aluminum (σ =17.6 MSm^{-1}, μ_r=1) and stainless steel (σ =1.38 MSm^{-1}, μ_r=1), the frequency range 5–15 Hz is not applied to these materials according to (2) and (4) at thickness near to 10 mm. Whether or not an applicable frequency range exits awaits further study.

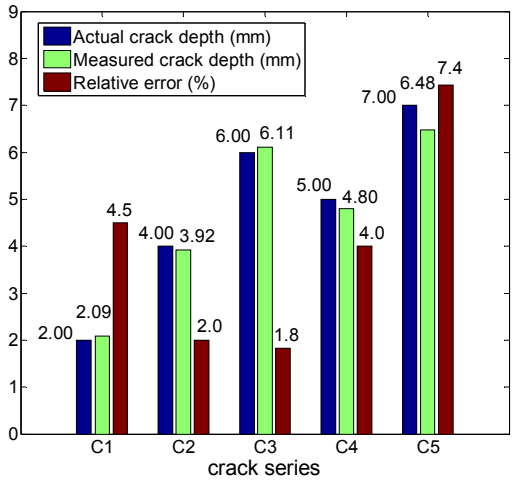

Fig.9. Comparative of actual and measured crack depth.

5. Conclusion

In summary, we used COMSOL to compute theoretical formulae and analyzed the redistribution current. A novel method that can solve bottom crack depth by using a simple mathematic equation based on finite element analysis was proposed and verified experimentally. The simulation and experiment results showed that:

(i) Multi-frequency range: f_{DC}~f_{SP} is valid in bottom crack measurement.

(ii) In the depth measurement of magnetic material crack, the ratio V_C/V_R varies linearly with f in a certain frequency range (like 5-15Hz) belonging to f_{DC}~f_{SP}.

(iii) The relation between crack depth d and the inverse of slope k is obtained.

(iv) The experiment results are in good agreement with fitting equation based on simulation.

It should be noted that this study has only detailed the bottom cracks which are perpendicular to bottom surface and the line between current injected electrodes, and it would be better to further modify equation (12) from a series of experiments and develop a comprehensive equation for both magnetic and non-magnetic materials. There are still some other factors to be taken into consideration, such as the crack orientation and location However, the issues are in our further study plan and may be solved by neural learning algorithm based on the redistribution current at the bottom crack tip studied in this paper. And how crack width affects the depth test using the proposed method is in our future work as well.

ACKNOWLEDGEMENT

This work was supported by the National Natural Science Foundation of China (Grant Nos. 61271329 and 51105260).

REFERENCES

[1] Hamia, R., Cordier, C., Dolabdjian, C. (2014). Eddy-current non-destructive testing system for the determination of crack orientation. *NDT & E International*, 61, 24-28.

[2] Tian, G.Y., Sophian, A. (2005). Defect classification using a new feature for pulsed eddy current sensors. *NDT & E International*, 38 (1), 77-82.

[3] Heidari, T., Seidfaraji, H., Sadeghi, S.H.H., et al. (2013). A fast analysis technique for electromagnetic interaction of high-frequency AC current-carrying wires with arbitrary-shape cracks in ferrous metals. *IEEE Transactions on Magnetics*, 49 (3), 1101-1107.

[4] Zhang, J., Drinkwater, B.W., Wilcox, P.D., et al. (2010). Defect detection using ultrasonic arrays: The multi-mode total focusing method. *NDT & E International*, 43 (2), 123-133.

[5] Merah, N. (2003). Detecting and measuring flaws using electric potential techniques. *Journal of Quality in Maintenance Engineering*, 9 (2), 160-175.

[6] Bowler, N., Huang, Y. (2005). Model-based characterization of homogeneous metal plates by four-point alternating current potential drop measurements. *IEEE Transactions on Magnetics*, 41 (6), 2102-2110.

[7] Lu, Z.J., Nicholas, P.J., Evans, W.J. (1995). Calibration of an ACPD monitoring system for small crack growth in corner crack specimens. *Engineering Fracture Mechanics*, 50 (4), 443-456.

[8] Saguy, H., Rittel, D. (2005). Bridging thin and thick skin solutions for alternating currents in cracked conductors. *Applied Physics Letters*, 87 (8), 084103.

[9] Venkatsubramanian, T.V., Unvala, B.A. (1984). An AC potential drop system for monitoring crack length. *Journal of Physics E: Scientific Instruments*, 17 (9), 765.

[10] Bowler, N. (2011). Four-point potential drop measurements for materials characterization. *Measurement Science and Technology*, 22 (1), 012001.

[11] Wheeler, H.A. (1942) Formulas for the skin effect. *Proceedings of the IRE*, 30 (9), 412-424.

[12] Sposito, G., Cawley, P., Nagy, P.B. (2010). An approximate model for three-dimensional alternating current potential drop analyses using a commercial finite element code. *NDT & E International*, 43 (2), 134-140.

[13] Raja, M.K., Mahadevan, S., Rao, B.P.C, et al. (2010). Influence of crack length on crack depth measurement by an alternating current potential drop technique. *Measurement Science and Technology*, 21 (10), 105702.

[14] Lewis, A.M., Michael, D.H., Lugg, M.C., et al. (1988). Thin skin electromagnetic fields around surface breaking cracks in metals. *Journal of Applied Physics*, 64 (8), 3777-3784.

[15] Sposito, G., Cawley, P., Nagy, P.B. (2010). Potential drop mapping for the monitoring of corrosion or erosion. *NDT & E International*, 43 (5), 394-402.

[16] Kawakam, Y., Kanaji, H., Oku, K. (2011). Study on application of field signature method (FSM) to fatigue crack monitoring on steel bridges. *Procedia Engineering*, 14, 1059-1064.

[17] Kim, Y.C., Asa, Y., Oku, K. (2007). Monitoring of initiation and propagation of fatigue cracks in steel plate deck by FSM. *Quarterly Journal of the Japan Welding Society*, 25 (4), 542-547.

[18] Hwang, I.S. (1992). A multi-frequency AC potential drop technique for the detection of small cracks. *Measurement Science and Technology*, 3 (1), 62.

[19] Saguy, H., Rittel, D. (2006). Alternating current flow in internally flawed conductors: A tomographic analysis. *Applied Physics Letters*, 89 (9), 094102.

[20] Saguy, H., Rittel, D. (2007). Application of ac tomography to crack identification. *Applied Physics Letters*, 91 (8), 084104.

[21] Pryor, R.W. (2011). *Multiphysics Modeling Using COMSOL: A First Principles Approach*. Ontario, Canada: Jones & Bartlett Publishers.

Received June 10, 2015.
Accepted October 07, 2015.